



PERGAMON

Chemical Engineering Science 56 (2001) 2357–2370

Chemical
Engineering Science

www.elsevier.nl/locate/ces

Analytical and numerical solutions describing the inward solidification of a binary melt

Daniel L. Feltham*, John Garside

Department of Chemical Engineering, University of Manchester Institute of Science and Technology (UMIST), P.O. Box 88, Manchester M60 1QD, UK

Abstract

We present a mathematical model describing the inward solidification of a slab, a circular cylinder and a sphere of binary melt kept below its equilibrium freezing temperature. The thermal and physical properties of the melt and solid are assumed to be identical. An asymptotic method, valid in the limit of large Stefan number \mathcal{S} , is used to decompose the moving boundary problem for a pure substance into a hierarchy of fixed-domain diffusion problems. Approximate, analytical solutions are derived for the inward solidification of a slab and a sphere of a binary melt which are compared with numerical solutions of the unapproximated system. The solutions are found to agree within the appropriate asymptotic regime of large Stefan number and small time. Numerical solutions are used to demonstrate the dependence of the solidification process upon the level of impurity and other parameters. We conclude with a discussion of the solutions obtained, their stability and possible extensions and refinements of our study. © 2001 Elsevier Science Ltd. All rights reserved.

Keywords: Phase change; Diffusion; Heat conduction; Transient response; Interface

1. Introduction

Solidification problems have applications in many fields of scientific and technological endeavour and have been the focus of extensive study. They are interesting both because of the diversity of their application and because of their nonlinearity, which is associated with the moving interface. In this paper, we focus on the solidification (freezing) of binary melts which are, at least initially, *undercooled* (also known as *supercooled*), by this we mean that the temperature of the melt lies *below* its equilibrium freezing temperature. The problem treated is the determination of the evolution of the temperatures, composition and solid–melt interface during the inward solidification of an undercooled binary melt in which one of the components is preferentially rejected from the forming solid phase. We consider the solidification from one side of a finite slab and the spherically symmetric inward solidification of a sphere from its surface. The surfaces from which solidification commences are held at

a constant temperature throughout the solidification process. These problems have many areas of application, most obviously to the casting of metal structures in moulds but also, for example, to the prilling process (Buttiker, 1981). The inward solidification of slabs, circular cylinders and spheres of pure melts at their freezing temperature has received considerable attention, for example Tao (1967), Pedroso and Domoto (1973), Stewartson and Waechter (1976), Poots (1962), Riley, Smith, and Poots (1974), Soward (1980) and Gupta (1987). Much of the work for circular cylinders and spheres has been in deriving asymptotic series solution methods which can deal with singularities in the final stages of solidification. Our problem differs from these in that the melt is initially taken to be undercooled and the freezing temperature is taken to be dependent upon the composition. This means that the temperature and composition within the melt is determined as part of the solution. Solidification of binary alloys in semi-infinite domains has been considered by Worster (1986), who used similarity solutions, and by Crowley and Ockendon (1979), who used an enthalpy formulation with numerical solution using a finite difference scheme. Solidification into an undercooled pure melt is typically highly unstable and the presence of a second component often

* Corresponding author. Present address: Centre of Polar Observation and Modelling, Department of Space and Climate Physics, UCL, Gower Street, London WC1E 6BT, UK.

exacerbates the instability, Langer (1980); the result of this is the formation of a highly convoluted, dendritic, solid–melt interface. That the surface from which solidification commences is undercooled, however, stabilises the solid–melt interface so that it may remain planar throughout. We discuss this matter in Section 7.

In Section 2, we present a nondimensional mathematical model of the inward solidification process and adopt a coordinate scaling which serves to fix the domain of integration. In Section 3, we present an asymptotic series expansion which has the effect of decomposing the problem into a sequence of fixed domain, linear diffusion problems. In Section 4, we solve these equations for the inward solidification of a finite slab and a sphere and draw attention to a problem in determining the composition. In Section 5, we present a similarity solution suitable for describing the small-time behaviour of the composition within the melt in a slab. In Section 6, numerical solutions are presented which are compared with our analytical results. In Section 7, we demonstrate the dependence of our solutions upon parameters and discuss stability in the light of the Mullins–Sekerka instability, Mullins and Sekerka (1964). Concluding remarks are presented in Section 8 with some suggestions for extending the study.

2. Mathematical formulation

The geometry of the problem is depicted in Fig. 1. Initially the slab or sphere is completely molten with constant undercooling and is in thermodynamic equilibrium with the surroundings which are held at the same temperature throughout. The melt is unstable at this temperature and we assume that nucleation takes place at one face of the slab or the surface of the sphere and solidification then proceeds inward with a flat (slab) or spherical (sphere) interface. As solidification proceeds, latent heat is released which diffuses into the melt and back to the boundary while the non-solidifying component is rejected and diffuses into the melt. The heat and component released into the melt cannot escape, thus the temperature and composition (concentration) of the melt increase as solidification proceeds. Since the average temperature of the melt increases and its temperature profile flattens due to diffusion, heat loss from the solidification front to the surroundings dominates heat loss into the melt. If the temperature of the surroundings lies above the melt's eutectic temperature then the increase in composition within the melt will eventually reduce its liquidus (freezing) temperature to that of the surroundings. At this point, undercooling within the melt is eliminated and solidification ceases, leaving a molten region. If the temperature of the surroundings is equal to or less than the eutectic temperature then the melt will solidify completely.

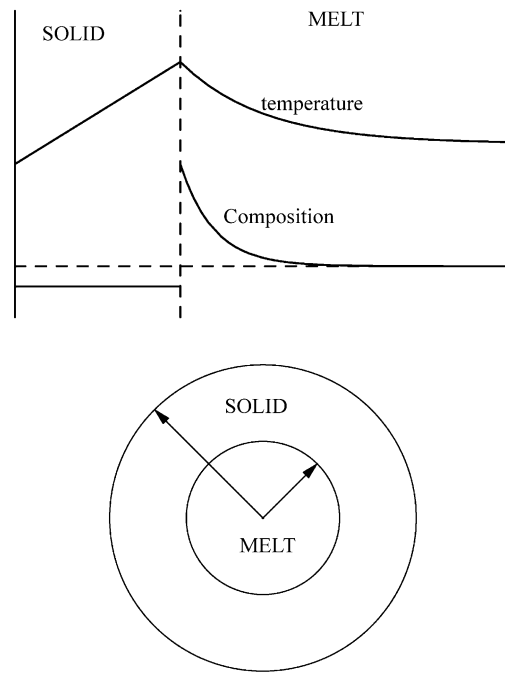


Fig. 1. The geometry of the problem that we consider: (a) depicts schematic temperature and composition profiles through the slab or cross-section of the cylinder and sphere; (b) depicts the phase regions in a cross-section of the cylinder and sphere.

We adopt a continuum model of this solidification process: The temperatures and compositions determined from the model represent quantities which are averaged over a volume much smaller than diffusion lengthscales and the domain size but which is large enough to contain many of the particles which constitute the material. We non-dimensionalise our equations using the domain length L (the slab length or sphere radius) as our length scale and L^2/κ as our time scale, where κ is the thermal diffusivity. We shall assume that the thermal and physical properties of the solid and melt are identical. We do this primarily for mathematical tractability since, although the assumption can be relaxed, it makes the mathematical analysis (and especially the analytical work) significantly more involved. Provided that the density change upon solidification (typically involving contraction) is not too great, the qualitative conclusions drawn from our analysis are valid. If the density change is large, however, and results, for example, in the formation of significant voids or fracturing of the solid region, a considerably detailed, material-specific model would need to be developed and numerical methods employed. We make no predictions in such cases. The effect of different diffusivities in the solid and melt will be to alter the magnitude of heat conduction in those regions but, since heat is still extracted from the binary melt to the surroundings, there are no qualitative implications for the solutions presented in this paper. If the thermal diffusivity of the solid

region is *significantly* smaller than that of the melt, there may be a *short* time during which heat flux from the solid–melt interface is dominated by the conduction into the melt. The heat flux into the solid will soon dominate, however, as the temperature of the melt rises and its temperature gradient weakens. The equations describing local conservation of heat and composition within the melt and solid regions are

$$\frac{\partial u_1}{\partial t} = \frac{1}{x^m} \frac{\partial}{\partial x} \left(x^m \frac{\partial u_1}{\partial x} \right) \quad (0 \leq x \leq s), \quad (1)$$

$$\frac{\partial v_1}{\partial t} = \frac{1}{x^m} \frac{1}{Le} \frac{\partial}{\partial x} \left(x^m \frac{\partial v_1}{\partial x} \right) \quad (0 \leq x \leq s), \quad (2)$$

$$\frac{\partial u_2}{\partial t} = \frac{1}{x^m} \frac{\partial}{\partial x} \left(x^m \frac{\partial u_2}{\partial x} \right) \quad (s \leq x \leq 1). \quad (3)$$

In these equations, $s(t)$ is the position of the solid–melt interface, x is the distance from the centre of the sphere or distance from the non-solidifying slab face and t is time. The parameter m is either 0, 1 or 2 according to whether we consider a slab, circular cylinder or sphere, respectively; in the latter two cases we assume the problem is radially symmetric. The dimensionless temperatures are

$$u_i = \frac{T_i - T_{in}}{T_L(C_{in}) - T_{in}} \quad (i = 1, 2), \quad (4)$$

where $i = 1$ refers to the melt and $i = 2$ refers to the solid region, respectively. These dimensionless values are related to the dimensional temperatures T_i , the initial temperature and composition of the melt, T_{in} and C_{in} , respectively, and the liquidus (freezing) temperature at the initial composition, $T_L(C_{in})$. The dimensional composition within the solid region is taken to be very small and is represented by the constant $C_s \approx 0$, the dimensionless composition within the melt and solid regions are

$$v_1 = \frac{C_1 - C_{in}}{C_{in} - C_s}, \quad v_2 = -1, \quad (5)$$

where C_1 is the dimensional composition in the melt. The parameter appearing in the compositional diffusion equation is the Lewis number,

$$Le = \frac{\kappa}{D}, \quad (6)$$

the ratio of thermal diffusivity κ to compositional diffusion coefficient D .

These diffusion equations are subject to the following boundary conditions. At the non-solidifying face of the slab and along the central axis of a circular cylinder and centre of the sphere, we impose the condition

$$\frac{\partial u_1}{\partial x} = 0, \quad \frac{\partial v_1}{\partial x} = 0 \quad (m = 0), \quad u_1, v_1 \text{ remain finite} \\ (m \neq 0) \quad (x = 0). \quad (7)$$

This condition prevents heat and composition from diffusing from the non-solidifying face of the slab and prevents a discontinuity at $x = 0$ for the circular cylinder or sphere. At the solid–melt interface, the temperature is given by the equilibrium freezing temperature, the liquidus. This implies that solidification takes place in a state of near equilibrium, which is justified except where solidification is extremely rapid and/or the radius of the sphere or cylinder is extremely small (where surface energy plays a role). The liquidus temperature is dependent upon the composition and we assume that this dependence is locally linear so that $T_L(C_1) = T_L(C_1 = 0) - \Gamma^* C_1$, where Γ^* is a positive (dimensional) constant. Non-dimensionally, we write the temperature at the solid–melt interface as

$$u_1 = 1 - \mathcal{C} v_1 \quad (x = s), \quad (8)$$

where the compositional ratio is

$$\mathcal{C} = \frac{C_{in} - C_s}{C_L(T_{in}) - C_{in}} \quad (9)$$

and $C_L(T_{in})$ is the liquidus composition at the given initial temperature. We consider $C_s \approx 0$ and, for an initial undercooling, $C_{in} < C_L(T_{in})$; typically $\mathcal{C} \ll 1$. Conservation of energy across the solid–melt interface gives us the Stefan condition,

$$\frac{ds}{dt} = \frac{1}{\mathcal{S}} \left(\frac{\partial u_2}{\partial x} - \frac{\partial u_1}{\partial x} \right) \quad (x = s), \quad (10)$$

where \mathcal{S} is the Stefan number,

$$\mathcal{S} = \frac{\mathcal{L}}{c_p(T_L(C_{in}) - T_{in})} \quad (11)$$

with latent heat \mathcal{L} and specific heat capacity c_p . The Stefan number represents a balance between the latent heat and the sensible heat deficit of the initial undercooling. The Stefan condition (10) shows that the latent heat released or absorbed by phase change is balanced by the heat flux into and out of the solid–melt interface. As solidification proceeds, composition is expelled from the forming solid phase. Conservation of composition across the interface yields

$$(1 + v_1) \frac{ds}{dt} = - \frac{1}{Le} \frac{\partial v_1}{\partial x} \quad (x = s). \quad (12)$$

Our final boundary condition is the requirement that the face of the slab from which solidification commences and the surface of the cylinder or sphere is at the same temperature as the surroundings, T_{in} . Non-dimensionally, the condition is

$$u_2 = 0 \quad (x = 1). \quad (13)$$

The specification of the problem is completed with our initial data

$$u_1 = 0, \quad v_1 = 0, \quad s = 1 \quad (t = 0). \quad (14)$$

that is the slab, cylinder and sphere is initially completely molten and uniformly undercooled.

The diffusion equations (1)–(3), and the conditions (7), (8), (10), (12)–(14) are a closed mathematical system. The evolution of the temperatures, composition and solid–melt interface are dependent upon the three parameters \mathcal{S} , Le and \mathcal{C} . In many melts and especially aqueous melts, these parameters take extreme values: $\mathcal{S} \gg 1$, $Le \gg 1$ (see, for example, Huppert, 1990). In our analytical studies, we shall consider $\mathcal{C} \ll 1$ which is true for almost pure systems such as those generated in the production of industrial or medical compounds.

Analysis of this system is complicated by the geometrical non-linearity of the moving solid–melt interface. This non-linearity is rendered explicit by using a boundary fixing coordinate transformation (Crank, 1984). This introduces a quasi-advection term into the governing diffusion equations. Introduction of the scaled coordinates

$$\zeta_1 = \frac{x}{s(t)}, \quad \zeta_2 = \frac{x-1}{s(t)-1} \quad (15)$$

allows us to rewrite the equations describing the system as

$$s^2 \frac{\partial u_1}{\partial t} - \zeta_1 s \frac{ds}{dt} \frac{\partial u_1}{\partial \zeta_1} = \frac{1}{\zeta_1^m} \frac{\partial}{\partial \zeta_1} \left(\zeta_1^m \frac{\partial u_1}{\partial \zeta_1} \right), \quad (16)$$

$$s^2 \frac{\partial v_1}{\partial t} - \zeta_1 s \frac{ds}{dt} \frac{\partial v_1}{\partial \zeta_1} = \frac{1}{Le} \frac{1}{\zeta_1^m} \frac{\partial}{\partial \zeta_1} \left(\zeta_1^m \frac{\partial v_1}{\partial \zeta_1} \right), \quad (17)$$

$$(s-1)^2 \frac{\partial u_2}{\partial t} - \zeta_2 (s-1) \frac{ds}{dt} \frac{\partial u_2}{\partial \zeta_2} = \frac{1}{((s-1)\zeta_2 + 1)^m} \frac{\partial}{\partial \zeta_2} \left(((s-1)\zeta_2 + 1)^m \frac{\partial u_2}{\partial \zeta_2} \right), \quad (18)$$

$$\frac{\partial u_1}{\partial \zeta_1} = 0, \quad \frac{\partial v_1}{\partial \zeta_1} = 0 \quad (m=0),$$

$$u_1, v_1 \text{ remain finite } (m \neq 0) \quad (\zeta_1 = 0), \quad (19)$$

$$u_1 = 1 - \mathcal{C}v_1, \quad \frac{ds}{dt} = \frac{1}{\mathcal{S}} \left(\frac{1}{(s-1)} \frac{\partial u_2}{\partial \zeta_2} - \frac{1}{s} \frac{\partial u_1}{\partial \zeta_1} \right),$$

$$(1+v_1) \frac{ds}{dt} = -\frac{1}{Le} \frac{1}{s} \frac{\partial v_1}{\partial \zeta_1} \quad (\zeta_1 = \zeta_2 = 1), \quad (20)$$

$$u_2 = 0 \quad (\zeta_2 = 0), \quad (21)$$

$$u_1 = 0, \quad v_1 = 0, \quad s = 1 \quad (t = 0), \quad (22)$$

where ζ_1, ζ_2 each span the domain $[0,1]$.

3. Asymptotic analysis

Consider the system of equations (16)–(22). Since the Stefan number is typically large, we see from the Stefan

condition that the solid–melt interface advances at a rate much slower than that at which the temperature fields evolve within the melt and solid. This suggests an asymptotic solution based upon expansions in $\varepsilon = 1/\sqrt{\mathcal{S}} \ll 1$. We expand all of the dependent variables as asymptotic series in ε ,

$$u_i = u_{i,0} + \varepsilon u_{i,1} + \varepsilon^2 u_{i,2} + \dots \quad (i=1,2), \quad (23)$$

$$v_1 = v_{1,0} + \varepsilon v_{1,1} + \varepsilon^2 v_{1,2} + \dots, \quad (24)$$

$$s = 1 + \varepsilon s_1 + \varepsilon^2 s_2 + \dots \quad (25)$$

A further simplification is obtained by considering the case that $\mathcal{C} \ll 1$, so that the freezing temperature is little affected by small to moderate values of the composition. We consider

$$\mathcal{C} = \bar{\mathcal{C}} \varepsilon^q, \quad (26)$$

where $\bar{\mathcal{C}}$ is of $\mathcal{O}(1)$. The value of $q \geq 2$ is chosen so that the dependence of the temperature upon the composition is removed up to $\mathcal{O}(\varepsilon^q)$. In this case, the determination of the temperatures in the melt and solid regions proceeds in the same way as for the solidification of a pure substance. The temperature gradients are then used to calculate the position and speed of the solid–melt interface, which are used to determine the composition within the melt.

Substituting these expressions into the governing equations and boundary conditions, using standard series expansions where appropriate, and equating like powers of ε yields a sequence of differential problems. To $\mathcal{O}(\varepsilon^0)$, we have

$$\frac{\partial u_{1,0}}{\partial t} = \frac{1}{\zeta_1^m} \frac{\partial}{\partial \zeta_1} \left(\zeta_1^m \frac{\partial u_{1,0}}{\partial \zeta_1} \right), \quad (27)$$

$$\frac{\partial v_{1,0}}{\partial t} = \frac{1}{Le} \frac{1}{\zeta_1^m} \frac{\partial}{\partial \zeta_1} \left(\zeta_1^m \frac{\partial v_{1,0}}{\partial \zeta_1} \right), \quad (28)$$

$$0 = \frac{\partial^2 u_{2,0}}{\partial \zeta_2^2}, \quad (29)$$

$$\frac{\partial u_{1,0}}{\partial \zeta_1} = 0, \quad \frac{\partial v_{1,0}}{\partial \zeta_1} = 0 \quad (m=0),$$

$$u_{1,0}, v_{1,0} \text{ remain finite } (m \neq 0) \quad (\zeta_1 = 0), \quad (30)$$

$$u_{1,0} = 1, \quad \frac{ds_1}{dt} = \frac{1}{s_1} \frac{\partial u_{2,0}}{\partial \zeta_2}, \quad 0 = -\frac{1}{Le} \frac{\partial v_{1,0}}{\partial \zeta_1}$$

$$(\zeta_1 = \zeta_2 = 1), \quad (31)$$

$$u_{2,0} = 0 \quad (\zeta_2 = 0), \quad (32)$$

$$u_{1,0} = 0, \quad v_{1,0} = 0, \quad s_1 = 0 \quad (t = 0). \quad (33)$$

This problem is linear, the diffusion equations are homogeneous and the boundary conditions are independent of time; it admits solution by means of Laplace transforms and eigenfunction expansions in the usual way. To $\mathcal{O}(\varepsilon)$,

we have

$$\frac{\partial u_{1,1}}{\partial t} - \frac{1}{\zeta_1^m} \frac{\partial}{\partial \zeta_1} \left(\zeta_1^m \frac{\partial u_{1,1}}{\partial \zeta_1} \right) = \zeta_1 \frac{ds}{dt} \frac{\partial u_{1,0}}{\partial \zeta_1} - 2s_1 \frac{\partial u_{1,0}}{\partial t}, \quad (34)$$

$$\frac{\partial^2 u_{2,1}}{\partial \zeta_2^2} = -ms_1 \frac{\partial u_{2,0}}{\partial \zeta_2}, \quad (35)$$

$$\frac{\partial u_{1,1}}{\partial \zeta_1} = 0 \quad (m = 0), \quad u_{1,1} \text{ remains finite } (m \neq 0) \quad (\zeta_1 = 0), \quad (36)$$

$$u_{1,1} = 0, \quad \frac{ds_2}{dt} = \frac{1}{s_1} \frac{\partial u_{2,1}}{\partial \zeta_2} - \frac{s_2}{s_1^2} \frac{\partial u_{2,0}}{\partial \zeta_2} - \frac{\partial u_{1,0}}{\partial \zeta_1} \quad (\zeta_1 = \zeta_2 = 1), \quad (37)$$

$$u_{2,1} = 0 \quad (\zeta_2 = 0), \quad (38)$$

$$u_{1,1} = 0, \quad s_2 = 0 \quad (t = 0), \quad (39)$$

where we have omitted the expressions for the composition field in light of the discussion presented in the next section. This problem is linear but the governing diffusion equations are inhomogeneous. The diffusion equations have been written such that their right-hand sides are known functions of position and time, obtained from the solutions of the previous order. Since the domain is simple, this inhomogeneity is most easily accommodated by using Green's functions. Note that the interface position is determined to one order higher than the other dependent variables.

The general expressions defining the $\mathcal{O}(\varepsilon^p)$ problem ($p < q$) are easily obtained (after lengthy algebra); the problem is inhomogeneous with terms which can be calculated from the previous orders. In principle, therefore, it is possible to calculate successively improved approximations by solutions of sets of diffusion problems with inhomogeneous body heating terms. In practice, however, these calculations become unwieldy; in the next section we calculate solutions only up to $\mathcal{O}(\varepsilon)$.

4. Solution of the perturbation equations

In the next two Sections we obtain solutions of the perturbation equations for the finite slab and sphere up to $\mathcal{O}(\varepsilon)$; the calculations for the circular cylinder proceed similarly.

4.1. The finite slab, ($m = 0$)

We work first to leading order. Results presented by Carslaw and Jaeger (1959) may be manipulated to yield the temperature in the melt $u_{1,0}$; using Laplace Transforms and the Inversion theorem the solution is obtained

to be

$$u_{1,0} = \sum_{n=0}^{\infty} (-1)^n \left\{ \operatorname{erfc} \left(\frac{2n+1-\zeta_1}{2t^{1/2}} \right) + \operatorname{erfc} \left(\frac{2n+1+\zeta_1}{2t^{1/2}} \right) \right\}, \quad (40)$$

where $\operatorname{erfc}(x)$ is the complementary error function, $\operatorname{erfc}(x) = 1 - \operatorname{erf}(x)$, where

$$\operatorname{erf}(x) = \frac{2}{\sqrt{\pi}} \int_0^x e^{-s^2} ds \quad (41)$$

is the error function. The temperature in the solid region is the stationary-state profile $u_{2,0} = \zeta_2$ and the composition within the melt is found to be $v_{1,0} = 0$.

The solid–melt interface is determined from $s_1' = 1/s_1$ where $s_1(0) = 0$; this has the physically relevant solution $s_1 = -\sqrt{2t}$.

We now proceed to $\mathcal{O}(\varepsilon)$. The Green's function satisfying the boundary conditions for the temperature in the melt $u_{1,1}$ has been obtained by Carslaw and Jaeger (1959) using the free-space Green's function, Laplace transforms and the inversion theorem to be

$$K(\zeta_1, t; \zeta, \tau) = 2 \sum_{n=1}^{\infty} \cos(\alpha_n \zeta_1) \cos(\alpha_n \zeta) \times \exp(-\alpha_n^2(\tau - t)), \quad (42)$$

where $\alpha_n = \pi/2 + n\pi$. Green's theorem now yields the solution as

$$u_{1,1}(\zeta, \tau) = \int_0^\tau \int_0^1 g(\zeta_1, t) K d\zeta_1 dt, \quad (43)$$

where

$$g(\zeta_1, t) = \zeta_1 \frac{ds_1}{dt} \frac{\partial u_{1,0}}{\partial \zeta_1} - 2s_1 \frac{\partial u_{1,0}}{\partial t} = \sum_{n=0}^{\infty} \frac{(-1)^n}{\sqrt{2\pi t}} \left\{ (-3\zeta_1 + 4n + 2) \times \exp\left(-\frac{(2n+1-\zeta_1)^2}{4t}\right) + (3\zeta_1 + 4n + 2) \times \exp\left(-\frac{(2n+1+\zeta_1)^2}{4t}\right) \right\}. \quad (44)$$

The double integral in the expression for $u_{1,1}$ must be performed using numerical quadrature for each point $\{\zeta, \tau\}$. Inclusion of five terms in a partial sum approximation for each of K and g was found to be satisfactory. The temperature in the solid is found to be $u_{2,1} = 0$.

Substituting for the known functions, the equation determining the position of the solid–melt interface is

$$\frac{ds_2}{dt} - \frac{1}{2t} s_2 = f(t), \quad (45)$$

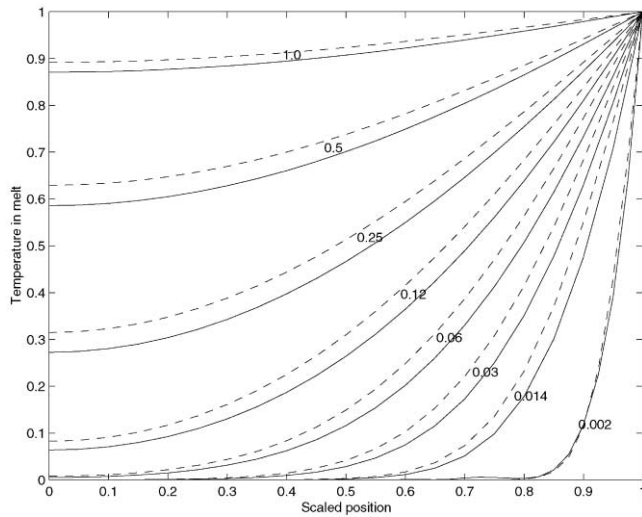


Fig. 2. Plots of $u_{1,0}$ for the slab. The solid line is the regular perturbation solution and is obtained analytically; the dashed line includes the pseudo-advection term arising from the singularity in s_1 ; it is obtained numerically. The numbers on the plots indicate time in dimensionless units.

where $s_2(0) = 0$ and

$$f(t) = - \sum_{n=0}^{\infty} \frac{(-1)^n}{\sqrt{\pi t}} \{e^{-n^2/t} - e^{-(n+1)^2/t}\}. \quad (46)$$

The solution is

$$s_2(t) = t^{-1/2} \int_0^t z^{1/2} f(z) dz. \quad (47)$$

Since $ds_1/dt = -1/\sqrt{2t}$, there is potentially a problem with our asymptotic approach as $t \rightarrow 0$. In this limit, $\epsilon ds_1/dt$ is no longer asymptotically small and it is appropriate to include the pseudo-advection term

$$- \zeta_1 \epsilon \frac{ds_1}{dt} \frac{\partial u_{1,0}}{\partial \zeta_1} \quad (48)$$

in the left-hand side of Eq. (27). A similar term must be included in Eq. (28) and the boundary condition expressing conservation of composition at the solid–melt interface (31) should be replaced with

$$(1 + v_{1,0})\epsilon \frac{ds_1}{dt} = - \frac{1}{Le} \frac{\partial v_{1,0}}{\partial \zeta_1}. \quad (49)$$

It is only by considering these modified equations that we can determine the effect of excluding the movement of the solid–melt interface on the $\mathcal{O}(\epsilon^0)$ solutions. In Fig. 2, we plot the analytical expression for $u_{1,0}$ as determined above (the dashed line) with the numerical solution of the modified differential problem (solid line) with $\mathcal{S} = 10$. The numerical solution was obtained using NAG routine D03PCF with a spatial step of 1/599 and a time step of 5×10^{-6} . Here, and throughout this paper, the numbers

on the plots indicate time in dimensionless units. We see from this that excluding the pseudo-advection term has only a moderate effect on the leading order approximation. This is to be expected since, although the pseudo-advection term transports heat very rapidly initially, it becomes negligible for times $t > \epsilon^2/2$. The role of the pseudo-advection term is more prominent in determining the composition, however, since it appears in the boundary condition (49). Effectively, in the time $0 < t < \epsilon^2/2$, composition is released into the melt which renders the solution $v_{1,0} = 0$ invalid. It is not trivial to find an approximate, analytical expression for the composition within the melt. In the next section, we present a similarity solution for the composition within a semi-infinite melt which may be used to approximate the composition field for very small times.

Since $s_1 = -\sqrt{2t}$, we expect the asymptotic series to lose its asymptoticness for times of $\mathcal{O}(\frac{1}{2}\epsilon^{-2})$, since for these times $\epsilon s_1 \sim 1$; this affects the expressions for the temperature fields also since these depend upon s .

4.2. The sphere, ($m = 2$)

Again, we start by working to leading order. The problem determining the temperature in the melt $u_{1,0}$ is transformed into a diffusion problem on a rod using the well-known transformation $\theta_{1,0} = \zeta_1 u_{1,0}$. This yields

$$\frac{\partial \theta_{1,0}}{\partial t} = \frac{\partial^2 \theta_{1,0}}{\partial \zeta_1^2}, \quad (50)$$

$$\theta_{1,0} = 0 \quad (\zeta_1 = 0), \quad (51)$$

$$\theta_{1,0} = 1 \quad (\zeta_1 = 1), \quad (52)$$

$$\theta_{1,0} = 0 \quad (t = 0). \quad (53)$$

The solution for $u_{1,0} = \theta_{1,0}/\zeta_1$ is found, using eigenfunction expansions, to be

$$u_{1,0} = 1 + \frac{1}{\zeta_1} \sum_{j=1}^{\infty} e^{-j^2 \pi^2 t} \frac{2}{j\pi} (-1)^j \sin(j\pi \zeta_1). \quad (54)$$

The temperature in the solid is the stationary-state profile $u_{2,0} = \zeta_2$. The composition within the melt $v_{1,0} = 0$, but the comments made above apply. As before, we obtain $s_1 = -\sqrt{2t}$.

We now proceed to $\mathcal{O}(\epsilon)$. Utilising the transformation $\theta_{1,1} = \zeta_1 u_{1,1}$, we see that the temperature in the melt is determined from

$$\frac{\partial \theta_{1,1}}{\partial t} - \frac{\partial^2 \theta_{1,1}}{\partial \zeta_1^2} = g_s(\zeta_1, t), \quad (55)$$

$$\theta_{1,1} = 0 \quad (\zeta_1 = 0, 1), \quad (56)$$

$$\theta_{1,1} = 0 \quad (t = 0), \quad (57)$$

where

$$g_s(\zeta_1, t) = \frac{ds_1}{dt} \left(\zeta_1 \frac{\partial \theta_{1,0}}{\partial \zeta_1} - \theta_{1,0} \right) - 2s_1 \frac{\partial \theta_{1,0}}{\partial t} \quad (58)$$

$$= \sum_{j=1}^{\infty} e^{-j^2 \pi^2 t} \frac{2(-1)^j}{j\pi} \left\{ -\frac{j\pi \zeta_1}{\sqrt{2t}} \cos(j\pi \zeta_1) + \left(\frac{1 - 4tj^2 \pi^2}{\sqrt{2t}} \right) \sin(j\pi \zeta_1) \right\}. \quad (59)$$

The Green's function for this problem is obtained using images of the free-space Green's function K_F ,

$$K(\zeta_1, t; \zeta, \tau) = \sum_{n=-\infty}^{\infty} \{ K_F(\zeta_1, t; \zeta + 2n, \tau) - K_F(\zeta_1, t; -\zeta + 2n, \tau) \}, \quad (60)$$

where

$$K_F(\zeta_1, t; \zeta, \tau) = \frac{H(\tau - t)}{\sqrt{4\pi L e(\tau - t)}} \exp\left(-\frac{(\zeta_1 - \zeta)^2}{4L e(\tau - t)} \right) \quad (61)$$

and $H(\tau - t)$ is the Heaviside function: $H(\tau - t) = 1$ for $\tau \geq t$, $H(\tau - t) = 0$ for $\tau < t$. The ($n \neq 0$) and $K_F(\zeta_1, t; -\zeta, \tau)$ terms in the expression for K are the images of each other and of $K_F(\zeta_1, t; \zeta, \tau)$ and serve to satisfy the boundary conditions. The solution is obtained to be

$$u_{1,1}(\zeta, \tau) = \frac{1}{\zeta} \int_0^{\tau} \int_0^1 K g_s(\zeta_1, t) d\zeta_1 dt. \quad (62)$$

The double integral in this expression is evaluated in the same way as that for $u_{1,1}$ in the slab but more terms are needed in the partial sum approximations of K and g_s , especially for very small times (20 terms were used for $\tau = 0.002$). The temperature in the solid region is readily determined to be

$$u_{2,1} = \sqrt{2t}(\zeta_2^2 - \zeta_2). \quad (63)$$

The position of the solid–melt interface is given, after substitution of the known functions, by

$$\frac{ds_2}{dt} + \frac{1}{2t}s_2 = f_s(t) - 2, \quad (64)$$

where $s_2(0) = 0$ and

$$f_s(t) = \sum_{j=1}^{\infty} e^{-j^2 \pi^2 t} \frac{2}{j\pi} (-1)^j \{ \sin(j\pi) - j\pi \cos(j\pi) \}. \quad (65)$$

The solution is

$$s_2 = t^{-1/2} \int_0^t z^{1/2} (f_s(z) - 2) dz. \quad (66)$$

5. Similarity solution describing the composition within the melt for a semi-infinite slab

Consider a semi-infinite slab of melt, with the position of the inward solidification front prescribed as $s(t) = \lambda t^{1/2}$. Composition is expelled as solidification proceeds, we seek to determine the composition within the slab. The perturbation analysis of the preceding section motivates setting $\lambda = \sqrt{2/\mathcal{L}}$. The problem can be expressed in terms of a similarity variable $\eta = \zeta t^{-1/2}$ as

$$-\frac{1}{2}\eta \frac{\partial v}{\partial \eta} = \frac{1}{Le} \frac{\partial^2 v}{\partial \eta^2} \quad (\eta > \lambda), \quad (67)$$

$$(1+v) \frac{1}{2} \lambda = -\frac{1}{Le} \frac{\partial v}{\partial \eta} \quad (\eta = \lambda), \quad (68)$$

$$v \rightarrow 0 \quad (\eta \rightarrow \infty) \quad (69)$$

and the initial data ($v = 0$ at $t = 0$) is automatically satisfied. This ordinary differential problem yields a solution by repeated integration,

$$v(\eta) = \frac{\lambda \operatorname{erfc}(\sqrt{Le}\eta/2)}{\exp(-\lambda^2 Le/4)/\sqrt{\pi} - \lambda \operatorname{erfc}(\sqrt{Le}\lambda/2)}. \quad (70)$$

Expressing this solution for our finite domain requires the replacement $\eta \rightarrow 1 - \eta$. This solution is compared with the numerical solution of the composition field in the finite slab in the next section.

6. Numerical and analytical solutions

Before comparing analytical and numerical solutions for the slab and sphere, we describe how we solve the unapproximated problem (16)–(22) numerically. The spatial dependence of the quasi-advection–diffusion equations determining u_1 , u_2 and v_1 is discretised in order to generate a system of coupled ordinary differential equations in time. The solid–melt interface $s(t)$ appears in these equations and is determined from the Stefan condition, the second of Eq. (20). The temperature gradients at the interface in the Stefan condition are approximated using a second-order method found to be satisfactory in a study by Furzeland (1980) (which does not involve a fictitious point). This is used to yield an ordinary differential equation for $s(t)$, which is coupled to the equations for the temperature and composition. The system is solved using the NAG routine D03PCF, which handles the spatial discretisation and solves the resulting system of stiff ordinary differential equations. The benefit of using the boundary-fixing coordinate transformation is now clear: it eliminates the need to track the solid–melt interface between grid points.

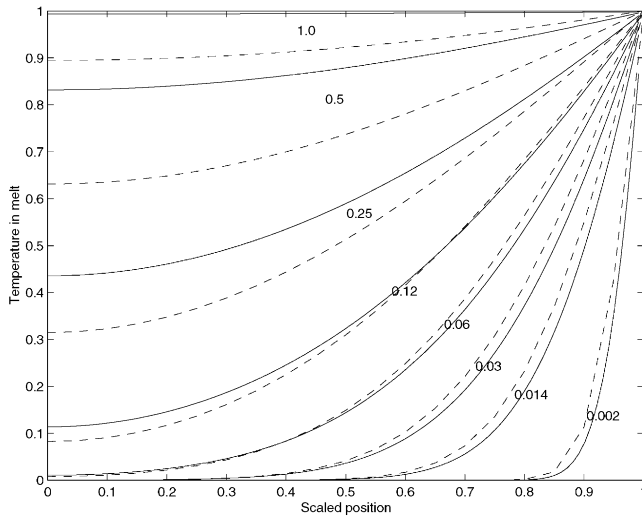


Fig. 3. The temperature in the melt with $\mathcal{S} = Le = 10$, $\mathcal{C} = 10^{-3}$, slab. The solid line is the numerical solution and the dashed line is the analytical solution. The numbers on the plots indicate time in dimensionless units.

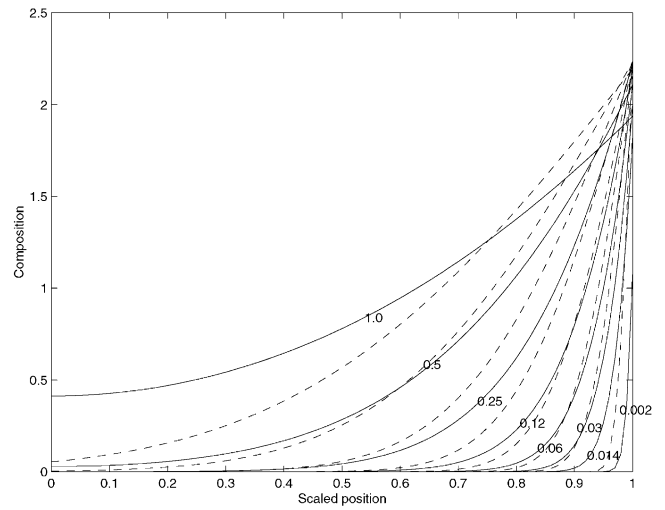


Fig. 5. The composition within the melt with $\mathcal{S} = Le = 10$, $\mathcal{C} = 10^{-3}$, slab. The solid line is the numerical solution and the dashed line is the similarity solution. The numbers on the plots indicate time in dimensionless units.

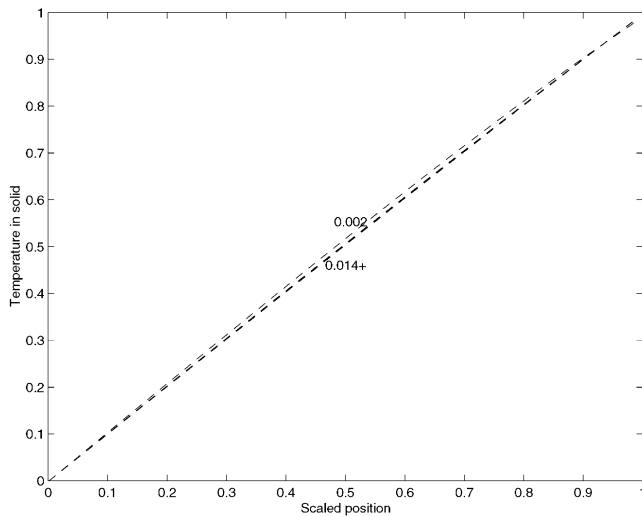


Fig. 4. The temperature in the solid region with $\mathcal{S} = Le = 10$, $\mathcal{C} = 10^{-3}$, slab. The plots were obtained numerically, the analytical solution is $u_2 = \zeta_2$. The numbers on the plots indicate time in dimensionless units.

6.1. The slab

In Figs. 3–5, we show the temperatures in the melt and solid regions and the composition within the melt; we have taken $\mathcal{S} = Le = 10$ and $\mathcal{C} = 10^{-3}$ with $N = 600$ spatial steps and a time step $\Delta t = 5 \times 10^{-6}$. For the temperature plots, the solid lines are the numerical solutions and the dashed lines the analytical solutions determined in the preceding section. Since $\varepsilon = 1/\sqrt{\mathcal{S}} \sim \frac{1}{3}$, we are near to the limit of validity of the asymptotic approxi-

mation. For small times ($t \ll 1$), the analytical solution for the temperature in the melt is clearly a good approximation but it breaks down for larger times, which is consistent with the breakdown of asymptoticness mentioned in Section 4 and the largeness of ε . The match between the numerical solution and the asymptotic solution (within the region of its applicability) lends confidence to both solutions. The similarity solution for the composition within the melt does not match the numerical solution particularly well. This is because the spatial scaling for the finite domain cannot be incorporated satisfactorily into the similarity solution because this is defined on an infinite domain. As a check on the numerical solutions, the integrals $\int_0^1 v_1 d\zeta_1$ were calculated and found to agree (as expected by conservation of mass) with $(1 - s)/s$ to within 5%. The temperature within the solid region reaches quasi-stationary state very rapidly according to both the numerical and analytical solutions. In the scaled coordinates we have used, its gradient remains approximately constant, however

$$\frac{\partial u_2}{\partial x} \sim \frac{(1 - \mathcal{C}v_1(s, t))}{\varepsilon\sqrt{2t}} \tag{71}$$

In Fig. 6, we show the position of the solid–melt interface against time (for the same parameter values). Clearly the agreement between the numerical solution (solid line) and the asymptotic solution (dashed line) is very good and better than might be expected given the performance of the asymptotic expression for the temperature within the melt. The reason for this is that the approximation upon which the asymptotic solution for the interface

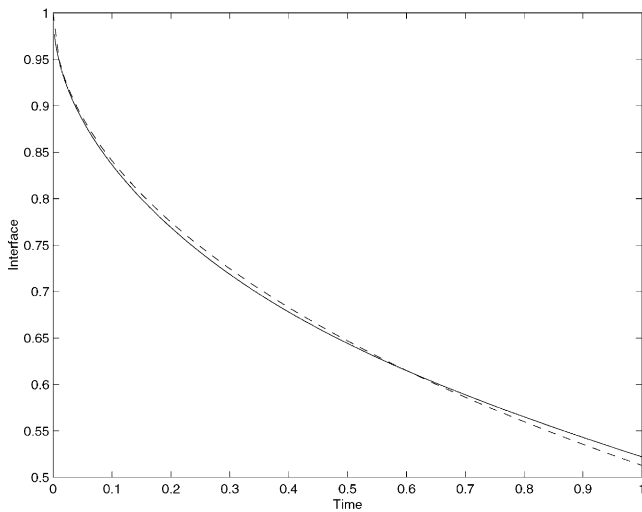


Fig. 6. Evolution of the solid–melt interface for the slab with $\mathcal{S} = Le = 10$, $\mathcal{C} = 10^{-3}$. The solid line is the numerical solution and the dashed line is the analytical solution.

relies, that the heat flux to the surroundings dominates that into the melt, is valid throughout the solidification process. At small times, the solid region is so thin that the temperature gradient across it is very steep and heat flux to the surroundings dominates. At later times, the temperature gradient in the solid is not so steep but heat flux to the surroundings still dominates since the temperature distribution within the melt has flattened and risen since heat is trapped within it and has diffused.

6.2. The sphere

It was found, for a wide range of spatial and temporal increments, that the NAG routine D03PCF failed to converge satisfactorily when dealing with the spherical equations and, in particular, failed to determine the solid–melt interface. In order to circumvent this, the spherical problem was transformed into an equivalent heat diffusion problem on a rod using the transformation $u_i = \theta_i/\zeta_i$, $v_1 = \Phi_1/\zeta_1$. In Figs. 7–9, we show the temperatures and composition in the melt obtained using this method for $\mathcal{S} = Le = 10$, $\mathcal{C} = 10^{-3}$, $N = 600$ and $\Delta t = 5 \times 10^{-6}$. Again, the composition profile within the melt was found to conserve mass to within 5%. The comments made above about the numerical and asymptotic solutions for the temperature and composition fields for the slab also apply for the inward solidification of a sphere. In Fig. 10, we show the interface position. The solid line is the numerical solution and the dashed line is the asymptotic approximation $1 + \varepsilon s_1$. We have neglected the term $\varepsilon^2 s_2$ since this is the modification due to the heat flux into the melt, which is negligible for larger times (where the analytical solution loses its asymptoticity).

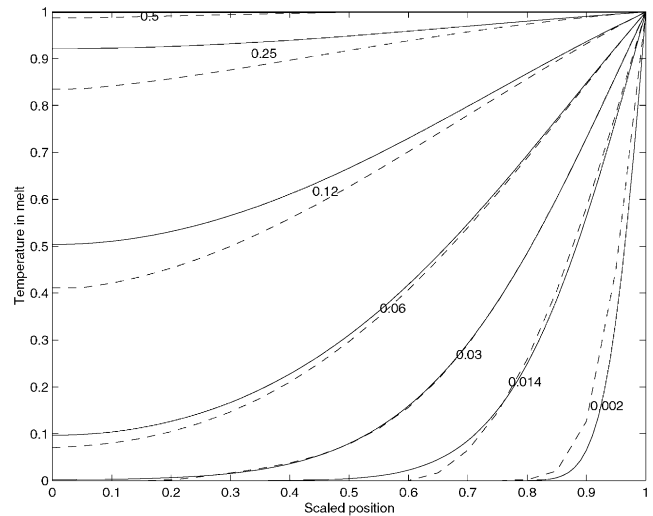


Fig. 7. The temperature in the melt with $\mathcal{S} = Le = 10$, $\mathcal{C} = 10^{-3}$, sphere. The solid line is the numerical solution and the dashed line is the analytical solution. The numbers on the plots indicate time in dimensionless units.

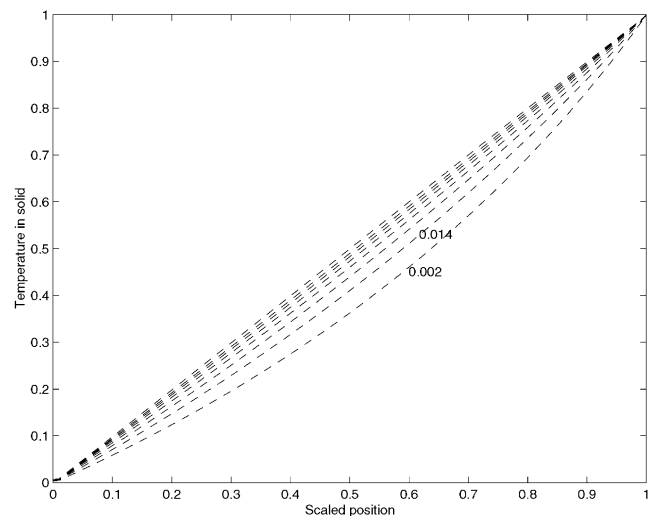


Fig. 8. The temperature in the solid region with $\mathcal{S} = Le = 10$, $\mathcal{C} = 10^{-3}$, sphere. The solutions were obtained numerically, the analytical solution is $u_2 = \zeta_2$. The numbers on the plots indicate time in dimensionless units.

7. Discussion

We have obtained solutions for the temperature, composition and position of the solid–melt interface for the inward solidification of an undercooled slab and sphere which depend upon the three dimensionless parameters \mathcal{S} , Le and \mathcal{C} . In the case that \mathcal{S} and \mathcal{C} take extreme values, we have obtained approximate, analytical solutions. The match between the analytical and numerical solutions lend confidence to the numerical method,

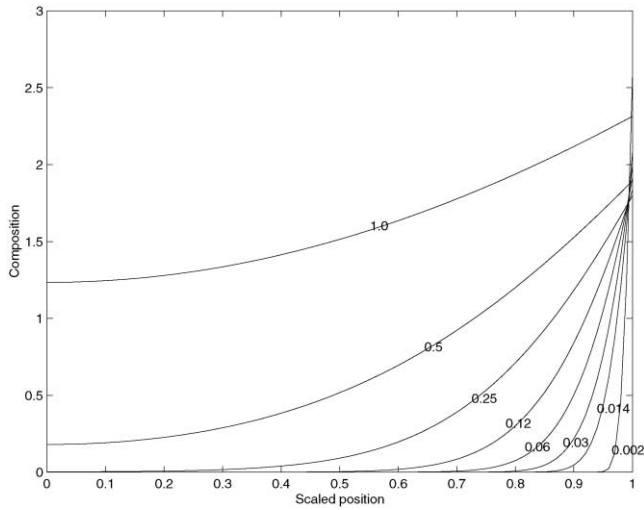


Fig. 9. The composition within the melt with $\mathcal{S} = Le = 10$, $\mathcal{C} = 10^{-3}$, sphere. The solutions were obtained numerically. The numbers on the plots indicate time in dimensionless units.

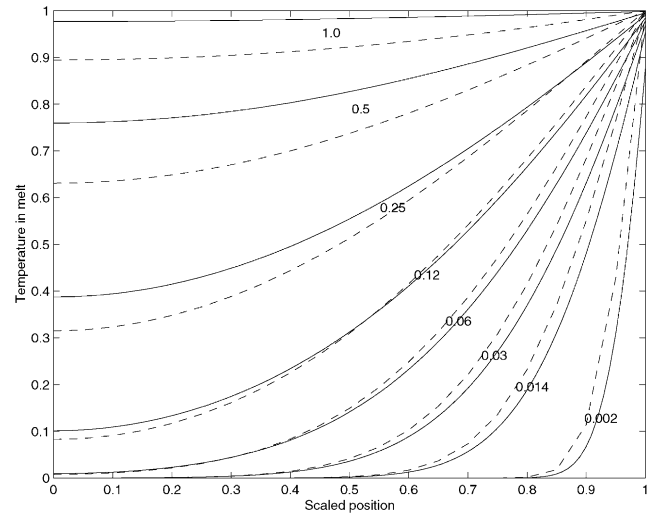


Fig. 11. The temperature in the melt with $\mathcal{S} = 20$, $Le = 10$, $\mathcal{C} = 10^{-3}$, slab. The solid line is the numerical solution and the dashed line is the analytical solution. The numbers on the plots indicate time in dimensionless units.

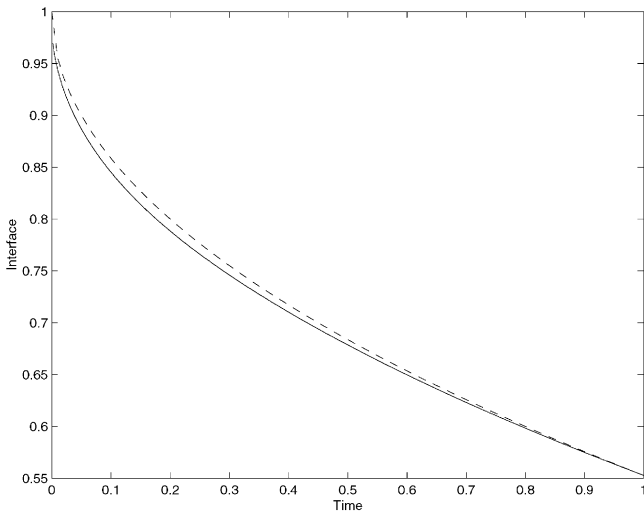


Fig. 10. Evolution of the solid–melt interface for the sphere with $\mathcal{S} = Le = 10$, $\mathcal{C} = 10^{-3}$. The solid line is the numerical solution and the dashed line is the analytical solution (neglecting $\varepsilon^2 s_2$).

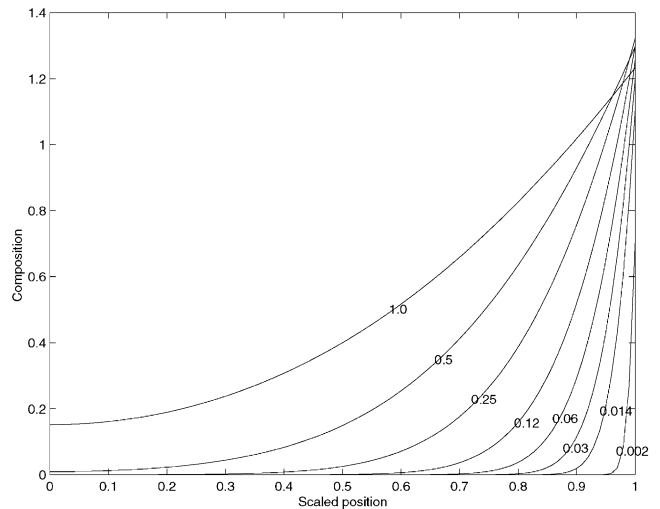


Fig. 12. The composition within the melt with $\mathcal{S} = 20$, $Le = 10$, $\mathcal{C} = 10^{-3}$, slab. The solutions were obtained numerically. The numbers on the plots indicate time in dimensionless units.

which may easily be used to explore the parameter dependence of the freezing process. In the interests of economy, we present a parametric study for the slab only. These conclusions also hold for the sphere.

Increasing the Stefan number \mathcal{S} is equivalent to decreasing the undercooling, causing the rate of solidification to decrease, and allowing the temperature and composition fields within the melt to more closely approach their quasi-stationary-state values (constants). An increase in \mathcal{S} also improves the accuracy of our analytical solutions and increases the length of time for which

they are asymptotic. Conversely, a decrease in the Stefan number has the opposite effect. This is partly illustrated by comparing the $\mathcal{S} = 10$ results with Figs. 11 and 12 which show sample plots of the temperature and composition in the molten region of the slab for $\mathcal{S} = 20$, $Le = 10$ and $\mathcal{C} = 10^{-3}$. Fig. 13 shows the variation of interface position for $\mathcal{S} = 10$ (solid line) and $\mathcal{S} = 20$ (dotted line) with $Le = 10$ and $\mathcal{C} = 10^{-3}$.

As the Lewis number Le approaches unity from above, the rate of diffusion of composition approaches the rate of diffusion of heat. In this case, numerical experiments

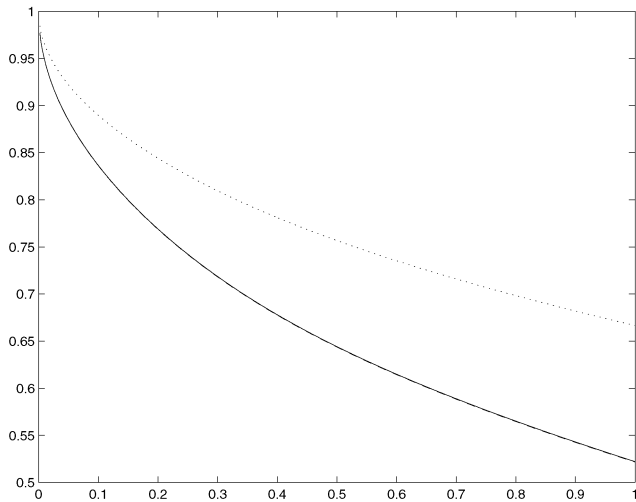


Fig. 13. Evolution of the solid-melt interface for the slab with $\mathcal{S} = 10$ (solid line) and $\mathcal{S} = 20$ (dotted line) with $Le = 10$, $\mathcal{C} = 10^{-3}$. The solutions were obtained numerically.

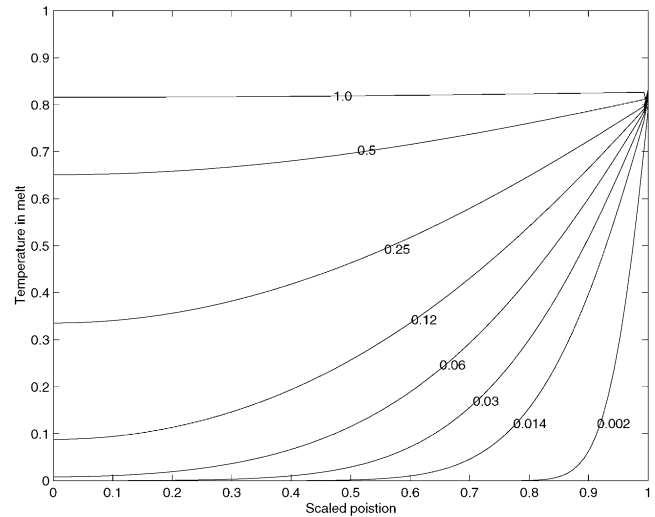


Fig. 15. The temperature in the melt with $\mathcal{C} = 10^{-1}$, $Le = 10$, $\mathcal{S} = 10$, slab. The solutions were obtained numerically. The numbers on the plots indicate time in dimensionless units.

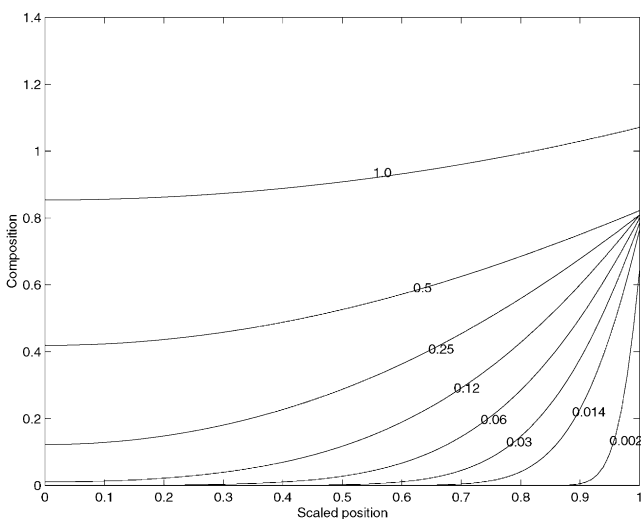


Fig. 14. The composition within the melt with $Le = 2$, $\mathcal{S} = 10$ and $\mathcal{C} = 10^{-3}$, slab. The solutions were obtained numerically. The numbers on the plots indicate time in dimensionless units.

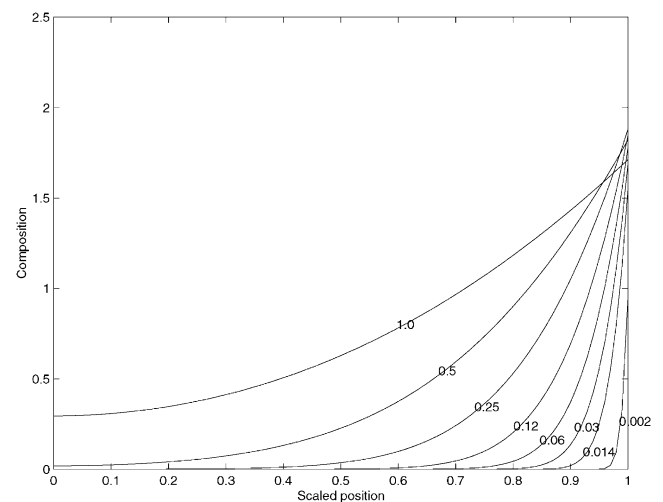


Fig. 16. The composition within the melt with $\mathcal{C} = 10^{-1}$, $Le = 10$, $\mathcal{S} = 10$, slab. The solutions were obtained numerically. The numbers on the plots indicate time in dimensionless units.

show (as one would expect) that the compositional boundary layer at the solid-melt interface widens, composition released upon solidification diffuses away more rapidly. This is illustrated by comparing Fig. 5 ($Le = 10$) with Fig. 14 which shows the composition in the molten region of the slab for $Le = 2$, $\mathcal{S} = 10$ and $\mathcal{C} = 10^{-3}$.

Figs. 15 and 16 show the temperature and composition within the molten region of the slab for $\mathcal{C} = 10^{-1}$, and are to be compared with Figs. 3 and 5 (which show the equivalent results for $\mathcal{C} = 10^{-3}$). From these plots, we see that an increase in the compositional ratio \mathcal{C} decreases

the solid-melt interfacial temperature which slows the rate at which solidification occurs and composition is released. In Fig. 17 we show the interface position for $\mathcal{C} = 10^{-3}$ (solid line), 10^{-2} (dashed line) and 10^{-1} (dotted line); the plots for $\mathcal{C} = 10^{-3}$ and 10^{-2} almost overlap but we see a substantial reduction in the extent of phase change for $\mathcal{C} = 10^{-1}$.

Let us consider how the final stage of the solidification process depends upon \mathcal{C} . We first consider a slab of melt for which $\mathcal{C} = 0$, in this case solidification proceeds as that for a pure medium. The temperature of the

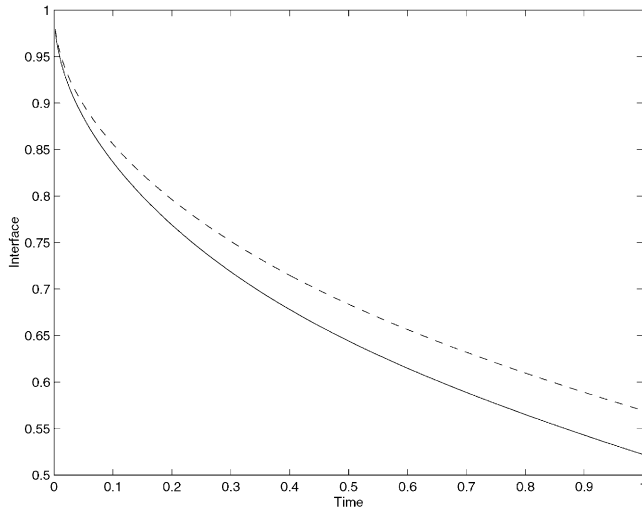


Fig. 17. Evolution of the solid–melt interface for the slab with $\mathcal{C} = 10^{-3}$, 10^{-2} (they overlap, the solid line) and $\mathcal{C} = 10^{-1}$ (dashed line) with $Le = 10$ and $\mathcal{S} = 10$. The solutions were obtained numerically.

solid–melt interface remains equal to the freezing temperature of the pure material ($u_i = 1$ at the interface), the temperature within the solid region is in a quasi-stationary state, $u_2 = \zeta_2$, and the temperature within the melt equals the freezing temperature, $u_1 = 1$. In this situation, the melt will solidify completely. At the point at which solidification completes, the temperature within the solid slab is given by $u_2 = \zeta_2$ except in a small region close to the newly solidified interface where the temperature profile flattens in order to satisfy the no-flux condition. The remaining sensible heat within the slab is transferred to the surroundings, so that finally the surroundings and slab are in equilibrium at the undercooling of the surroundings. Thus the final, stationary, stable state differs from the initial, stationary, unstable state only in that the melt has become completely solidified. Now, we consider the variation of our solution with \mathcal{C} . As \mathcal{C} increases, the effect of composition upon the liquidus (freezing) temperature of the melt becomes increasingly significant. The temperature of the solid–melt interface decreases, which decreases the rate of heat loss into the surroundings and slows solidification. Whatever the value of \mathcal{C} (provided that $\mathcal{C} \neq 0$), there will come a point at which the solid–melt temperature equals the surrounding temperature. Provided that the temperature of the surroundings lies above the eutectic, this will result in a residual molten region. If \mathcal{C} is of $\mathcal{O}(1)$ then solidification may cease (at $1 - \mathcal{C}v_1(\zeta_1 = 1) = 0$) almost immediately. We may define a critical compositional ratio from the similarity solution for the composition in the molten region of the slab (which is accurate near the interface for small times):

$$\mathcal{C}_{\text{crit}} = \frac{1}{v_1(\zeta_1 = 1)} = \sqrt{\frac{\mathcal{S}}{2\pi}} e^{-Le/(2\mathcal{S})} + \operatorname{erfc}\left(\sqrt{\frac{Le}{2\mathcal{S}}}\right). \quad (72)$$

For $\mathcal{S} = 10$ and $Le = 10$, $\mathcal{C}_{\text{crit}} = 0.4479$. For $\mathcal{S} \gg 1$ and $\mathcal{C} \ll \mathcal{C}_{\text{crit}}$, we expect the temperature and composition to reach their quasi-stationary values before freezing ceases. In this case, we can assume that $v_1 = (1 - s)/s$ so that solidification will cease once $1 - \mathcal{C}v_1 = 0$, which yields

$$s_{\infty} = \frac{\mathcal{C}}{1 + \mathcal{C}} \quad (73)$$

as the final dimension of the molten region. A similar argument applied to the inward solidification of a sphere leads to a molten region of size

$$s_{\infty}^{\circ} = \left(\frac{\mathcal{C}}{1 + \mathcal{C}}\right)^{1/3}. \quad (74)$$

For $\mathcal{C} = 10^{-3}$ – 10^{-1} the molten region in the slab is of negligible size $s_{\infty} \approx 10^{-3}$ – 0.09 ; however, an appreciable region may be left molten during the solidification of a sphere, $s_{\infty}^{\circ} \approx 0.1$ – 0.45 . An increase in \mathcal{C} will increase the size of the final molten region, although its size is always less than unity (some solidification always takes place). These arguments may easily be extended to determine an analytical approximation of the temporal dependence of the interface position. For $\mathcal{S} \gg 1$, $\mathcal{C} \ll \mathcal{C}_{\text{crit}}$ and t of $\mathcal{O}(1)$, $\dot{s} \sim (1 - \mathcal{C}v_q)/(\mathcal{S}(1 - s))$, where v_q is the quasi-stationary composition in the melt: $v_q = (1 - s)/s$ for the slab and $v_q = (1 - s^3)/s^3$ for the sphere. These nonlinear ordinary differential equations can be solved in implicit, but closed, form to satisfy an initial condition $s(t = t_i) = s_i$. Numerical experiments show that the expressions obtained are particularly useful for larger times $t > \mathcal{O}(1)$ where the initial condition at $t_i > 0$ is determined from a numerical integration of the full system.

A key assumption in determining our solutions was that the problem was one dimensional, thus the spherical problem was spherically symmetric and there was no variation in directions orthogonal to the direction of growth in the slab. If the solid–melt interface is unstable then it may become convoluted and adopt a dendritic structure, invalidating our solutions. The instability is caused by the thermodynamic drive to maximise expulsion of heat and composition from the forming solid phase, which is enhanced if the solid–melt interface increases its area (becomes dendritic). A condition for the onset of instability was determined by Mullins and Sekerka (1964). They performed a linear stability analysis of a planar solidification front advancing into a semi-infinite binary alloy at a constant rate. Although the geometry and time-dependence of their problem differs from that presented in this paper, we expect the fundamental physical mechanism to be the same. A rigorous analysis of the morphological stability of the solid–melt interface for the inward solidification problems presented here would be an interesting, though involved, new work. Such a study ought to consider differences in thermal diffusivity in the solid and melt regions. In his study of

the solidification of a semi-infinite binary alloy, Worster (1986) used the Mullins–Sekerka criterion to determine at which point the planar solidification front became dendritic. Once the Mullins–Sekerka criterion had been satisfied, Worster used a continuum model of the dendritic region, the mushy-layer model. In the absence of surface tension, and using our dimensionless variables, the Mullins–Sekerka criterion may be written as

$$\frac{\partial u_1}{\partial x} + \mathcal{C} \frac{\partial v_1}{\partial x} > -\frac{\partial u_2}{\partial x} \quad \text{for instability.} \quad (75)$$

Since we have taken $\mathcal{C} \ll 1$ and our solutions show that $-\partial u_2/\partial x \gg \partial u_1/\partial x$ (note the use of unscaled coordinates), the Mullins–Sekerka criterion suggests that the solutions obtained in this paper are stable. An increase in \mathcal{C} would both weaken the stabilising temperature gradient in the solid phase (by decreasing the temperature at the solid–melt interface) and, combined with a large Lewis number, increase the constitutionally induced undercooling in the melt. This would cause the second term in Eq. (75) to increase and the third term to decrease in magnitude. For suitably chosen parameters, the Mullins–Sekerka criterion suggests that the solid–melt interface will become unstable.

Another way for the solid–melt interface to become unstable would be for the temperature of the surroundings to increase after solidification had commenced. This would decrease the stabilising temperature gradient in the solid (decreasing the rate of solidification) and allow instability to occur. If the surroundings were raised to the liquidus temperature at the solid–melt interface, then the stabilising temperature gradient in the solid would be eliminated and we might expect solidification to proceed inward in the same manner as does outward solidification into an undercooled melt, Langer (1980). Such a process may be thought to occur, on a very slow timescale, during the inward solidification of molten rock. The build-up of impurity at the solid–melt interface at the onset of instability is a likely explanation of the attractive bands of colour and dendritic structure seen in many geodes.

8. Conclusions

A continuum model for the inward solidification of an undercooled binary melt has been presented. Approximate, analytical solutions and numerical solutions describing the solid–melt interface position and the temperature and composition fields have been obtained for a finite slab and sphere. The agreement between these solutions, within the appropriate asymptotic regime, lends confidence to them. Numerical solutions were used to determine the parameter dependence of the solidification process and especially the effect of increasing the level of impurity. The satisfaction of the Mullins–Sekerka

criterion (which was determined for a different geometry and time-dependence) suggests that the solutions obtained are physically stable and the potential for instability by the Mullins–Sekerka mechanism was highlighted. The solutions potentially have application to a number of solidifying systems, for example metal casting and lava solidification. The work presented in this paper suggests an investigation of the conditions required for morphological instability of the solid–melt interface.

Notation

T_i	temperature in melt ($i = 1$), solid ($i = 2$)
C_1, C_s	composition in melt, solid (almost zero)
u_i	dimensionless temperature in melt ($i = 1$), solid ($i = 2$)
v_1	dimensionless composition in melt
T_{in}, C_{in}	initial temperature, composition of melt
$T_L(C_{in})$	liquidus (freezing) temperature of melt with initial composition
$C_L(T_{in})$	liquidus composition of melt with initial temperature
κ, \mathcal{L}, c_p	thermal diffusivity, latent heat, specific heat capacity of solid and melt
$Le, \mathcal{C}, \mathcal{S}$	Lewis number, compositional ratio, Stefan number
\mathcal{C}_{crit}	critical size of compositional ratio
$L, L^2/\kappa$	lengthscale, time scale
x, t, s	distance, time, position of solid–melt interface
s_∞, s_∞°	final size of molten region for slab, sphere
m	parameter determining geometry: $m = 0$ slab; $m = 1$ circular cylinder; $m = 2$ sphere
K, K_F	Green's function, free space Green's function
$\text{erf}(\cdot), \text{erfc}(\cdot)$	error function, complementary error function
$H(\cdot)$	Heaviside function

Greek letters

ε	small parameter ($\varepsilon = 1/\sqrt{\mathcal{S}}$)
ζ_i	boundary-fixing spatial coordinates in melt ($i = 1$), solid ($i = 2$)
$u_{i,j}, v_{1,j}, s_j$	terms in asymptotic expansions
η	similarity variable ($\eta = \zeta t^{-1/2}$)
$\theta_{i,j}$	intermediate variable in calculation (temperature)

Acknowledgements

The authors acknowledge the financial support of Zeneca under the Strategic Research Fund scheme. One of us

(DLF) would particularly like to thank Grae Worster for useful discussions.

References

- Buttiker, R. (1981). Mechanism of particle formation during drying of free-falling drops containing solids. *German Chemical Engineering*, 4, 298–304.
- Carslaw, H. S., & Jaeger, J. C. (1959). *Conduction of heat in solids* (2nd ed.). Oxford Science Publications, Oxford: Oxford University Press.
- Crank, J. (1984). *Free and moving boundary problems*. Oxford Science Publications, Oxford: Oxford University Press.
- Crowley, A. B., & Ockendon, J. R. (1979). On the numerical solution of an alloy solidification problem. *International Journal of Heat and Mass Transfer*, 22, 941–946.
- Furzeland, R. M. (1980). A comparative study of numerical methods for moving boundary problems. *Journal of the Institute of Mathematical Applications*, 26, 411–429.
- Gupta, S. C. (1987). Analytical and numerical solutions of radially symmetric inward solidification problems in spherical geometry. *International Journal of Heat and Mass Transfer*, 30(12), 2611–2616.
- Huppert, H. E. (1990). The fluid mechanics of solidification. *Journal of Fluid Mechanics*, 212, 209–240.
- Langer, J. S. (1980). Instabilities and pattern formation in crystal growth. *Reviews of Modern Physics*, 52, 1–28.
- Mullins, W. W., & Sekerka, R. F. (1964). Stability of a planar interface during solidification of a dilute binary alloy. *Journal of Applied Physics*, 35(2), 444–451.
- Pedroso, R. I., & Domoto, G. A. (1973). Inward spherical solidification—solution by the method of strained coordinates. *International Journal of Heat and Mass Transfer*, 16, 1037–1043.
- Poots, G. (1962). On the application of integral-methods to the solution of problems involving the solidification of liquids initially at fusion temperature. *International Journal of Heat and Mass Transfer*, 5, 525–531.
- Riley, D. S., Smith, F. T., & Poots, G. (1974). The inward solidification of spheres and circular cylinders. *International Journal of Heat and Mass Transfer*, 17, 1507–1516.
- Soward, A. M. (1980). A unified approach to Stefan's problem for spheres and cylinders. *Proceedings of the Royal Society. London. Series A*, 373, 131–147.
- Stewartson, K., & Waechter, R. T. (1976). On Stefan's problem for spheres. *Proceedings of the Royal Society. London. Series A*, 348, 415–426.
- Tao, L. C. (1967). Generalised numerical solution of freezing a saturated liquid in cylinders and spheres. *A.I.Ch.E. Journal*, 13, 165–169.
- Worster, M. G. (1986). Solidification of an alloy from a cooled boundary. *Journal of Fluid Mechanics*, 167, 481–501.